Comparison of numerical methods for modeling laser mode locking with saturable gain

Shaokang Wang,* Andrew Docherty, Brian S. Marks, and Curtis R. Menyuk

Department of Computer Science and Electrical Engineering, University of Maryland Baltimore County, 1000 Hilltop Circle, Baltimore, Maryland 21250, USA
**Corresponding author: swan1@umbc.edu*

Received July 11, 2013; revised October 1, 2013; accepted October 1, 2013; posted October 2, 2013 (Doc. ID 193704); published October 31, 2013

The widely used split-step Fourier method has difficulties when solving partial differential equations with saturable gain. Here, we describe a modified split-step Fourier method, and we compare it to several different algorithms for solving the Haus mode-locking equation and related equations that are used to model mode-locked lasers and other optical oscillators and amplifiers with saturable gain. These equations all include the product of a scalar nonlinearity and a stiff nonlinear operator. We find that a modified split-step method is the easiest to program with the same level of reliability and accuracy as the other methods that we investigated.

OCIS codes: (000.4430) Numerical approximation and analysis; (140.3280) Laser amplifiers; (140.4050) Mode-locked lasers.
http://dx.doi.org/10.1364/JOSAB.30.003064

1. INTRODUCTION

Many optical systems contain saturable amplifiers with a band-limited gain. Some important examples include erbium-doped fiber amplifiers, mode-locked lasers, and optoelectronic oscillators. In general, the partial differential equation (PDE) that is used to model the system will have a term that is both nonlinear, due to the gain saturation, and stiff, due to the finite bandwidth of the amplifier. The solutions of these equations are more difficult to obtain than those for optical transmission systems, which do not have the coupling of nonlinearity and a band-limited frequency response. The split-step method is widely used to characterize light propagation in optical fibers because it is relatively easy to program. Moreover, prior work has demonstrated that it is efficient relative to other methods for studying optical transmission when a high accuracy is not needed [1]. However, there have not been comparable studies for mode-locked lasers and other related systems with saturable absorbers. As we show, stiffness enters into the equations that describe these systems in a way that is more difficult to handle accurately and efficiently than the way in which stiffness enters into the equations that describe transmission systems. With the introduction of frequency combs [2], the number of systems with saturable absorbers and their complexity has grown along with their potential applications. So a complete comparison of the computational methods for solving the equations that model these systems—comparable to what has been done for optical transmission systems—is needed.

In this paper, we investigate methods to solve initial value PDEs of the general form

$$\frac{\partial u}{\partial z} = \mathcal{L}u + g(u)\mathcal{K}u + \mathcal{N}(u,z), \tag{1}$$

where $u = u(z,t)$ is the complex carrier envelope of a scalar optical field, $\mathcal{L}$ and $\mathcal{K}$ are linear operators that are assumed to be stiff, $g(u)$ is a scalar nonlinear operator of the carrier envelope u, and $\mathcal{N}$ is a nonlinear operator that is not stiff. We use z as the evolution variable and t as the transverse variable, as is common when modeling optical systems.

In this paper, we use laser mode locking as our example application. The canonical equation in this context is the Haus mode-locking equation (HME) [3], which has also been commonly referred to in the literature as the master mode-locking equation [4,5] or the complex Ginzburg–Landau equation with saturable gain [6]. This PDE models the propagation of light pulses through a mode-locked laser and is of the form of Eq. (1). The effects of the discrete laser elements—nonlinear propagation, dispersion, gain, and saturable absorption—are averaged over one round trip in the laser cavity to give a continuous equation that qualitatively models all the physical effects necessary for passive, short-pulse laser mode locking,

$$\frac{\partial u}{\partial z} = -\frac{l}{2}u - \frac{i\beta''}{2}\frac{\partial^2 u}{\partial t^2} + \frac{g(u)}{2}\left(u + \frac{1}{\Omega_g^2}\frac{\partial^2 u}{\partial t^2}\right) + (i\gamma + \delta)|u|^2 u, \tag{2}$$

where t is the retarded time, z is the propagation distance, l is the loss, β'' is the group velocity dispersion, γ is the Kerr coefficient, Ω_g is the gain bandwidth, and δ is the fast saturable absorption constant. If the relaxation of the laser medium is much slower than the pulse repetition rate, the saturated gain is well approximated by

$$g(u) = \frac{g_0}{1 + P_{\mathrm{av}}(u)/P_{\mathrm{sat}}}, \tag{3}$$

where g_0 is the unsaturated gain, P_{sat} is the saturation power of the amplifier, and $P_{\text{av}}(u)$ is the average power of the pulse,

$$P_{\text{av}}(u) = \frac{1}{T_R}\int_{-T_R/2}^{T_R/2} |u(z,t)|^2 \mathrm{d}t, \tag{4}$$

in which T_R is the round-trip time. While Eq. (2) looks much like the nonlinear Schrödinger equation, it has complex instead of imaginary coefficients in front of the dispersive and nonlinear terms. These terms include the effects of a frequency filter and fast saturable absorption, respectively, and they are physically necessary in order to fix the central frequency of the mode-locked pulses and to suppress continuous waves. The slow saturable gain given in Eq. (3) suppresses explosive pulse growth. The correspondence between Eqs. (1) and (2) is given by

$$\mathcal{L} = -\frac{1}{2}\left(l + i\beta''\frac{\partial^2}{\partial t^2}\right), \tag{5a}$$

$$\mathcal{K} = \frac{1}{2}\left(1 + \frac{1}{\Omega_g^2}\frac{\partial^2}{\partial t^2}\right), \tag{5b}$$

$$\mathcal{N}(u,z) = (i\gamma + \delta)|u|^2 u. \tag{5c}$$

It is often useful to evaluate $\mathcal{L}$ and $\mathcal{K}$ in the Fourier domain, which then become

$$\tilde{\mathcal{L}} = (i\beta''\omega^2 - l)/2, \tag{6a}$$

$$\tilde{\mathcal{K}} = [1 - (\omega/\Omega_g)^2]/2, \tag{6b}$$

where ω is the frequency, and the tilde indicates the Fourier transform.

The nonlinear Schrödinger equation is the basic equation that describes nonlinear pulse propagation in optical fibers. Since it was first applied to optical fiber transmission by Hasegawa and Tappert [7], this equation and its extensions have been extensively studied in optical systems using numerical methods. Early finite-difference methods were found to be inferior to spectral methods—in particular, the split-step Fourier method, which was found to be the most numerically efficient method to solve the nonlinear Schrödinger equation [8,9].

Once we discretize the problem in the variable t, Eq. (1) is reduced to a system of ordinary differential equations (ODEs),

$$\frac{\mathrm{d}\mathbf{u}}{\mathrm{d}z} = \mathsf{L}\mathbf{u} + g(\mathbf{u})\mathsf{K}\mathbf{u} + \mathsf{N}(\mathbf{u},z), \tag{7}$$

where $\mathbf{u}$ is a vector of length N, with discretized elements $\mathbf{u}^{(j)}(z)$ approximating the solution at the time t_j, $j \in \{1,2,\ldots,N\}$. We have $T = N\Delta t$, where T is the duration of the time window in which $u(z,t)$ appears, and Δt is the discretized time step. We calculate the stationary pulse duration τ using the variance

$$\tau^2 = \frac{\int_{-T_R/2}^{T_R/2}(t-t_c)^2|u(z,t)|^2\mathrm{d}t}{\int_{-T_R/2}^{T_R/2}|u(z,t)|^2\mathrm{d}t}, \tag{8}$$

in which t_c is the center of the pulse

$$t_c = \frac{\int_{-T_R/2}^{T_R/2} t|u(z,t)|^2\mathrm{d}t}{\int_{-T_R/2}^{T_R/2}|u(z,t)|^2\mathrm{d}t}. \tag{9}$$

We verified that the evolution profile remains visibly the same (it is unchanged to at least three significant figures) when $20\tau \le T \le 60\tau$, as long as $\tau \ge 10\Delta t$. The matrices L and K are $N \times N$ matrices that are the discretization of the linear operators $\mathcal{L}$ and $\mathcal{K}$, respectively, and the nonlinear operator N is the discretization of $\mathcal{N}$. We will use the Fourier transform method to discretize the linear operators $\mathcal{L}$ and $\mathcal{K}$ in Eq. (1). We then approximate the integral in Eq. (4) by an inner product, so that

$$g(\mathbf{u}) = \frac{g_0}{1 + \mathbf{u}^H\mathbf{u}/E_0}, \tag{10}$$

where $\mathbf{u}^H$ is the complex transpose of the vector $\mathbf{u}$ and $E_0 = T_R P_{\text{sat}}/\Delta t$. The approximation of Eq. (10) is spectrally accurate; i.e., the error tends to zero exponentially as Δt decreases, as long as Fourier spectral methods are used [10]. That will be the case for the methods that we present in this paper.

Stiffness occurs when there are two or more very different scales of the propagation variable (in this case, z) on which the dependent variable (in this case, u) is changing [11]. The source of stiffness in Eq. (2) and the related equations is the second-order derivative in time t. If we consider the linear diffusive wave equation for $u(z,t)$ and its Fourier transform $\tilde{u}(z,\omega)$, we obtain

$$\frac{\partial u}{\partial z} = \frac{\partial^2 u}{\partial t^2}, \tag{11a}$$

$$\frac{\partial \tilde{u}}{\partial z} = -\omega^2\tilde{u}. \tag{11b}$$

When the time t is discretized for numerical computations, instability can result. As a simple illustration of how instability can appear, we may consider replacing Eq. (11) by its finite-difference version

$$\frac{\mathrm{d}\mathbf{u}^{(j)}}{\mathrm{d}z} = \frac{\mathbf{u}^{(j+1)} - 2\mathbf{u}^{(j)} + \mathbf{u}^{(j-1)}}{(\Delta t)^2}, \tag{12a}$$

$$\frac{\mathrm{d}\tilde{\mathbf{u}}^{(j)}}{\mathrm{d}z} = -\frac{\sin^2(\omega_j\Delta t)}{(\Delta t)^2}\tilde{\mathbf{u}}^{(j)}, \tag{12b}$$

where $\omega_j = 2(j-1)\pi/T$ is the discretized frequency. For any numerical method, the largest frequency that is retained in the problem is approximated by $\omega_{\max} = 2(N-1)\pi/T$. Equation (12b) predicts that the damping rate approaches zero at this frequency. The high-frequency components can then be made unstable by computational noise combined with nonlinear effects. We give an explicit example in Section 2.A. In the simple case shown here, the difficulty can be avoided by working in the Fourier domain, where we find

$\tilde{u}(z+\Delta z,\omega)=\tilde{u}(z,\omega)\exp(-\omega^2\Delta z)$, where Δz is the step size in the z direction. However, when $\omega^2\Delta z\sim 1$, we find $\Delta z\sim 1/\omega^2$, and the change $\tilde{u}(z+\Delta z,\omega)-\tilde{u}(z,\omega)$ is comparable to $\tilde{u}(z,\omega)$. The choice of Δt, and hence $\omega_{\max}$, imposes a constraint on how large Δz may be chosen while still maintaining computational accuracy and stability. This constraint can be quite serious and some computational methods will always be unstable due to the second derivative in t regardless of how small Δz is [12].

When the frequency filtering represented by the term $g(u)\partial^2 u/\partial t^2$ is not present, the stiffness enters in a relatively benign way, as is the case for most computational studies of optical waveguide transmission. When dispersion is present, we see from the solution to the dispersive wave equation

$$\frac{\partial u}{\partial z}=i\frac{\partial^2 u}{\partial t^2}, \tag{13a}$$

$$\frac{\partial \tilde{u}}{\partial z}=-i\omega^2\tilde{u}, \tag{13b}$$

which may be written as $\tilde{u}(z+\Delta z,\omega)=\tilde{u}(z,\omega)\exp(-i\omega^2\Delta z)$; that dispersion only changes the phase of the Fourier components. While the absolute magnitude of the change in $\tilde{u}$ for a given ω and z is the same for the diffusive and dispersive wave equation, and while one must be careful to avoid choices of Δz that lead to computational resonance [13], it is typically possible to tolerate far larger inaccuracies in phase than in amplitude while maintaining stability. However, for laser mode locking and other similar models, as we will show, the presence of the frequency filtering term $g(u)\partial^2 u/\partial t^2$ strongly affects the performance of the different computational methods that we will compare.

In this paper, we compare the split-step Fourier method to two newer algorithms, which are the additive Runge–Kutta (ARK) method of Kennedy and Carpenter [14], as well as the exponential time-differencing method of Cox and Matthews [15]. We analyze the computational efficiency and the stability of the algorithms when applied to solving the HME of Eq. (2). The remainder of this paper is organized as follows: Section 2 discusses in detail the implementation of the split-step method to solve saturable gain problems. Section 3 describes the application of the split-step method to the HME. Section 4 describes the implementation of the ARK method. Section 5 describes the exponential time-differencing method, and Section 6 shows the results of the comparison and discusses the relative merits of each method.

2. SPLIT-STEP FOURIER METHOD

Split-step methods have a long history going back to Strang [16] and Bagrinovskii and Godunov [17]. The simplest and most frequently used formulation is a second-order scheme, while schemes of arbitrarily high order were proposed by Yoshida [18]. The standard split-step method can be applied to Eq. (7) when the nonlinear-stiff term involving $g(\mathbf{u})$ is absent, so that we can split the equation into a stiff linear part represented by L and a nonstiff nonlinear part represented by $\mathsf{N}[u(z),z]$. Applying the standard second-order, symmetric split-step method to this modified problem would lead to the following formal expression for the numerical scheme:

$$\mathbf{u}_{k+1}=\exp(h\mathsf{L}/2)\exp\left(\int_{z_k}^{z_{k+1}}\mathsf{N}[\mathbf{u}(z'),z']\mathrm{d}z'\right)\exp(h\mathsf{L}/2)\mathbf{u}_k, \tag{14}$$

where $\mathbf{u}_k=\mathbf{u}(z_k)$, $z_{k+1}=z_k+h$, h is the size of the z step, and the nonlinear exponential is evaluated analytically when possible or is approximated numerically using a second-order explicit method. Furthermore, by using a Fourier spectral discretization, the linear exponential operators can often be efficiently calculated using the fast Fourier transform (FFT) [9,19]. When efficient use of a FFT is not possible—for example, if a Chebyshev spectral method is used [19]—the split-step method still has the advantage that the stiff part of the equation does not need to be solved implicitly.

The split-step method avoids stiffness by analytically solving the linear part of the equation, which is stiff, as in the case of the nonlinear Schrödinger equation [20]. However, for equations that have terms that are both stiff and nonlinear, as is the case for the HME with the term $g(\mathbf{u})\partial^2 u/\partial t^2$, and which often do not have analytical solutions, the application of a split-step method becomes difficult.

A. Symmetric Splitting

By applying a split-step scheme simplistically to Eq. (1), an intuitive scheme is

$$\mathbf{u}_{k+1}=\exp(h/2[\mathsf{L}+g(\mathbf{u}_k)\mathsf{K}])\exp\left(\int_{z_k}^{z_{k+1}}\mathsf{N}[\mathbf{u}(z'),z']\mathrm{d}z'\right)\times\exp(h/2[\mathsf{L}+g(\mathbf{u}_k)\mathsf{K}])\mathbf{u}_k, \tag{15}$$

where $g(\mathbf{u}_k)$ is the saturated gain that is calculated at the beginning of the kth step. With this approximation, $\exp\{h/2[\mathsf{L}+g(\mathbf{u}_k)]\mathsf{K}\}$ can be evaluated spectrally using the FFT, and stiffness is avoided since the discretized ODE is solved analytically. However, the saturated gain $g[\mathbf{u}(z)]$ is poorly approximated by a constant $g(\mathbf{u}_k)$ in each step, which makes this scheme first-order accurate.

Computational efficiency is the major concern in solving initial value problems numerically. A first-order method is generally inferior to a second-order method, since it is often necessary to take smaller step sizes to maintain a given global accuracy, which in turn requires more total computer time. This reduction in efficiency can seriously impact the usefulness of simulations for laser design, since it is often desirable to carry out parametric studies over a wide range. A similar issue arises in any model of a passively mode-locked laser with slow saturable gain.

The Richardson extrapolation is often used to formulate a higher-order result by combining lower-order estimates [21]. In the case of a first-order method, we formulate a second-order result by combining solutions with step sizes of h and $h/2$,

$$\mathbf{u}_{k+1}=2\mathbf{u}_{k+1}^{h/2}-\mathbf{u}_{k+1}^{h}, \tag{16}$$

where $\mathbf{u}_{k+1}^{h}$ is the first-order approximation of $\mathbf{u}(z_{k+1})$ using a step size of h. We will test the computational performance of the scheme in Eq. (16) against other methods.

To maintain second-order accuracy of the symmetric splitting, an alternative is to use a higher-order method to handle

all the nonlinear terms including the saturated gain. We would then compute

$$\mathbf{u}_{k+1} = \exp(h\mathsf{L}/2)\exp\left(\int_{z_k}^{z_{k+1}}\{g[\mathbf{u}(z')]\mathsf{K} + \mathsf{N}[\mathbf{u}(z'),z']\}\mathrm{d}z'\right) \times \exp(h\mathsf{L}/2)\mathbf{u}_k, \tag{17}$$

in which the linear term $\exp(h\mathsf{L}/2)$ can be handled analytically in the frequency domain. The integral of all the nonlinear terms can be evaluated by a second-order scheme when an analytical solution is not available, or, alternatively, by a nested splitting scheme when part of the integration is analytically solvable. In the case of Eq. (17), we may approximate the nonlinear integration by a nested splitting scheme

$$\exp\left(\int_{z_k}^{z_{k+1}}\{g[\mathbf{u}(z')]\mathsf{K} + \mathsf{N}[\mathbf{u}(z'),z']\}\mathrm{d}z'\right)\mathbf{u} \approx \mathbf{F}_N\left\{\exp\left(\int_{z_k}^{z_{k+1}} g[\mathbf{u}(z')]\mathsf{K}\mathrm{d}z'\right)\mathbf{F}_N(\mathbf{u})\right\}, \tag{18}$$

where $\mathbf{F}_N[\mathbf{u}(z_0)] = \exp(\int_{z_0}^{z_0+h/2}\mathsf{N}[\mathbf{u}(z'),z']\mathrm{d}z')$. In order to be computationally efficient, explicit methods are usually preferred to evaluate $\exp(\int_{z_k}^{z_{k+1}} g[\mathbf{u}(z')]\mathsf{K}\mathrm{d}z')$ when its analytical form is not available.

However, numerical instabilities are introduced when $\exp(\int_{z_k}^{z_{k+1}} g[\mathbf{u}(z')]\mathsf{K}\mathrm{d}z')$ is evaluated explicitly, since the second-order differentiation in t, which is similar to the diffusion term in Eq. (11), is stiff. In the case of the HME, we have

$$\exp\left(\int_{z_k}^{z_{k+1}} g(\mathbf{u})\mathsf{K}\mathrm{d}z'\right)\mathbf{u} \approx \mathrm{IFFT}\{[1 + hg(\mathbf{u})(1 - \omega^2/\Omega_g^2)/2]\mathrm{FFT}(\mathbf{u})\}, \tag{19}$$

which is stable only if $|1 + hg(\mathbf{u})(1 - \omega_{\max}^2/\Omega_g^2)/2| < 1$, where $\omega_{\max}$ is the largest frequency. So, the largest step size allowed is $h < 4[g(\mathbf{u})(\omega_{\max}^2/\Omega^2 - 1)]^{-1}$. Practical step sizes must be even smaller because of the presence of round-off errors. Although this stability analysis is based on Euler's method, which is a first-order explicit method, an instability of the same kind exists with any explicit method. The integration of terms that are both nonlinear and stiff, such as $\exp(\int_{z_k}^{z_{k+1}} g[\mathbf{u}(z')]\mathsf{K}\mathrm{d}z')$ in Eq. (2), always require special handling. We will explicitly show the appearance of this instability in Section 3.

B. Asymmetric Splitting

A different approach for handling the term that is proportional to $g(\mathbf{u})$ is needed to alleviate the stiffness, as well as to maintain good computational efficiency. We formulate a split-step scheme,

$$\mathbf{u}_{k+1} = \exp\left(h\mathsf{L}/2 + \left\{\int_{z_{k+1/2}}^{z_{k+1}} g[\mathbf{u}(z')]\mathrm{d}z'\right\}\mathsf{K}\right) \times \exp\left(\int_{z_k}^{z_{k+1}}\mathsf{N}[\mathbf{u}(z'),z']\mathrm{d}z'\right) \times \exp\left(h\mathsf{L}/2 + \left\{\int_{z_k}^{z_{k+1/2}} g[\mathbf{u}(z')]\mathrm{d}z'\right\}\mathsf{K}\right)\mathbf{u}_k, \tag{20}$$

in which the second-order derivative in t can be efficiently evaluated using the FFT. If we consider the function g to be function of z alone, $g(\mathbf{u}) \to g(z)$, we can approximate g with a Taylor series about z_k, $g(z) \simeq g(z_k) + g'(z_k)(z - z_k)$, where $g'(z) \equiv g'[\mathbf{u}(z)] = \mathrm{d}g[\mathbf{u}(z)]/\mathrm{d}z$. Evaluating the integrals that contain $g(z)$ in Eq. (20) using this approximation, we now can formally write the split-step method applied to the problem with saturable gain as

$$\mathbf{u}_{k+1} = \exp(\mathsf{L}h/2 + [g(z_{k+1/2}) + g'(z_{k+1/2})h/4]\mathsf{K}h/2) \times \exp\left(\int_{z_k}^{z_{k+1}}\mathsf{N}(\mathbf{u}(z'),z')\mathrm{d}z'\right) \times \exp(\mathsf{L}h/2 + [g(z_k) + g'(z_k)h/4]\mathsf{K}h/2)\mathbf{u}_k. \tag{21}$$

To extend this expansion to Eq. (7), we first expand $\mathbf{u}(z)$ in Taylor's series about z_k, so that

$$\mathbf{u}(z_k + \delta) \simeq \mathbf{u}(z_k) + \delta\left.\frac{\mathrm{d}\mathbf{u}}{\mathrm{d}z}\right|_{z=z_k}. \tag{22}$$

We then expand the function $g(\mathbf{u}_k + \delta\mathrm{d}\mathbf{u}_k/\mathrm{d}z)$ with δ small, so that we obtain a linear approximation for the gain

$$g(z_k + \delta) \simeq g(\mathbf{u}_k) + \delta J_g^H(\mathbf{u}_k)\frac{\mathrm{d}\mathbf{u}_k}{\mathrm{d}z} + \mathcal{O}(\delta^2), \tag{23}$$

where $\mathsf{J}_g(\mathbf{u}_k)$, which is a vector of length N, is the gradient of $g(\mathbf{u})$ evaluated at $\mathbf{u}_k$.

We now formally write the second-order split-step method for Eq. (7) using Eq. (23) as

$$\mathbf{u}_{k+1} = \exp(\mathsf{L}h/2 + [g(\mathbf{u}_{k+1/2}) + g_2(\mathbf{u}_k)h/4]\mathsf{K}h/2) \times \exp\left(\int_{z_k}^{z_{k+1}}\mathsf{N}[\mathbf{u}(z'),z']\mathrm{d}z'\right) \times \exp(\mathsf{L}h/2 + [g(\mathbf{u}_k) + g_2(\mathbf{u}_k)h/4]\mathsf{K}h/2)\mathbf{u}_k, \tag{24}$$

where

$$g_2(\mathbf{u}) = \mathsf{J}_g^H(\mathbf{u})\frac{\mathrm{d}\mathbf{u}}{\mathrm{d}z} = -\frac{2[g(\mathbf{u})]^2}{g_0E_0}\mathrm{Re}\{\mathbf{u}^H[\mathsf{L} + g(\mathbf{u})\mathsf{K}]\mathbf{u}\}, \tag{25}$$

and the exponential of the integral involving the nonlinear operator N can be evaluated analytically when possible or by using a second-order explicit method otherwise. This approach to splitting is asymmetric, and the nonlinear function $g_2(\mathbf{u})$ only has to be updated once each step to yield second-order accuracy. This scheme reduces to first-order splitting, as shown in Eq. (15), when we set $g_2(\mathbf{u}) = 0$.

Alternatively, we can also approximate the nonlinear integrations that involve the term with saturated gain in Eq. (20) iteratively [20]. This approach is equivalent to using a finite-difference approximation of $g'(\mathbf{u}_k) = \mathrm{d}g[\mathbf{u}(z)]/\mathrm{d}z|_{z=z_k}$,

$$g_2(\mathbf{u}_k) = \frac{1}{h/2}[g(\hat{\mathbf{u}}_{k+1/2}) - g(\mathbf{u}_k)], \tag{26}$$

where $\hat{\mathbf{u}}_{k+1/2}$ is a first-order approximation to $\mathbf{u}(z_{k+1/2})$, which may be written as

$$\hat{\mathbf{u}}_{k+1/2} = \exp[\mathsf{L}h/2 + g(\mathbf{u}_k)\mathsf{K}h/2]\mathbf{u}_k.$$

This scheme is also second-order accurate and can be used when the directional derivative of $g(\mathbf{u})$ cannot be calculated analytically. In the case of the HME, the formulation of Eq. (26) also provides a second-order correction similar to the formulation of Eq. (25), and we obtained nearly identical computational efficiency by applying the split-step method of Eq. (24) to the HME using these two different approaches for updating $g_2(\mathbf{u})$. Here, we will only show the result in Section 6 when the formalism of Eq. (25) is used.

The split-step algorithm of Eq. (24) is second order and does not perform as efficiently as fourth-order methods when the required errors become sufficiently small. Fourth-order versions of the split-step method have been given [18]; however, here we will use Richardson extrapolation to derive a method that is fourth-order accurate and has the additional advantage of giving lower-order estimates that can then be used to control the step size [1]. We combine the solutions with step sizes of h, $h/2$, and $h/4$ in the following way [21]:

$$\mathbf{u}_{k+1} = \frac{1}{21}(32\mathbf{u}_{k+1}^{h/4} - 12\mathbf{u}_{k+1}^{h/2} + \mathbf{u}_{k+1}^{h}), \tag{27}$$

in which $\mathbf{u}_{k+1}^{h}$ is a second-order approximation of $\mathbf{u}(z_{k+1})$ using the step-size h. To estimate the error and control the step size, we construct a third-order approximation in a similar fashion, and we use it to estimate the local error of the third-order estimate. We update h so that this error is held nearly constant [14].

3. APPLYING THE SPLIT-STEP METHOD TO THE HME

Equation 2 has a soliton solution with a special choice of parameters that has the following form [3]:

$$u(z,t) = A_0\,\mathrm{sech}^{1+i\beta}(t/\tau)\exp(i\phi z), \tag{28}$$

where the parameters of this solution, A_0, β, τ, and ϕ can be found by substituting Eq. (28) into Eq. (2). Two sets of parameters are given in Table 1. Parameter set 1 has been used to model a system with anomalous dispersion that can be considered as a perturbation of the nonlinear Schrödinger equation [4,22]. Parameter set 2 models a system with normal dispersion where both the gain and saturable loss have a large effect on the equation and cannot be considered to be perturbations.

Table 1. Two Sets of Normalized Parameters Used for Computing the HME Numerically

Parameter	Set 1	Set 2
g_0	0.4	3
β''	−2	3
l	0.2	2
γ	4	4
δ	0.03	1
$T_R P_{\mathrm{sat}}$	1	1
Ω_g	$\sqrt{10}$	$\sqrt{2}$
A_0	0.880	0.0759
τ	0.804	43.634
β	9.411×10^{-4}	5.110
ϕ	1.548	2.247×10^{-2}

For the HME, the nonlinear, nonstiff step of the split-step Fourier method can be evaluated either analytically or by using a second-order explicit method. Here, we use the analytical solution, which is given by

$$\exp\left[\int_0^h (\delta + i\gamma)|u(\zeta,t)|^2 u(\zeta,t)\mathrm{d}\zeta\right] = u(0,t)[1 - 2h\delta|u(0,t)|^2]^{-(\delta+i\gamma)/(2\delta)}. \tag{29}$$

Using the analytical solution for the nonlinear step in Eq. (29), the asymmetric split-step method is implemented as

$$\mathbf{u}_k^{\mathrm{i}} = \mathrm{IFFT}\{\exp[h(\tilde{\mathsf{L}} + g(\mathbf{u}_k)\tilde{\mathsf{K}})/2 + h^2 g_2 \tilde{\mathsf{K}}/8]\mathrm{FFT}[\mathbf{u}_k]\}, \tag{30a}$$

$$\mathbf{u}_k^{\mathrm{ii}} = \mathbf{u}_k^{\mathrm{i}}(1 - 2h\delta|\mathbf{u}_k^{\mathrm{i}}|^2)^{-(\delta+i\gamma)/(2\delta)}, \tag{30b}$$

$$\mathbf{u}_{k+1} = \mathrm{IFFT}\{\exp[h(\tilde{\mathsf{L}} + g(\mathbf{u}_k^{\mathrm{ii}})\tilde{\mathsf{K}})/2 + h^2 g_2 \tilde{\mathsf{K}}/8]\mathrm{FFT}[\mathbf{u}_k^{\mathrm{ii}}]\}, \tag{30c}$$

where we recall that a tilde indicates the Fourier transform. In the HME the differential operators L and K are implemented in the Fourier domain and are diagonal matrices

$$\tilde{\mathsf{L}}_{jj} = (i\beta''\omega_j^2 - l)/2, \tag{31}$$

$$\tilde{\mathsf{K}}_{jj} = [1 - (\omega_j/\Omega_g)^2]/2, \tag{32}$$

and the correction term g_2 in Eq. (30) is given by

$$g_2 = -\frac{2g^2(\mathbf{u}_k)}{g_0 N P_{\mathrm{sat}}}\,\mathrm{Re}\{[\mathrm{FFT}[\mathbf{u}_k]]^H[\tilde{\mathsf{L}} + g(\mathbf{u}_k)\tilde{\mathsf{K}}]\mathrm{FFT}[\mathbf{u}_k]\}. \tag{33}$$

We will also use the explicit expressions for L and K in the HME that are given in Eqs. (31) and (32) in Sections 4 and 5. A MATLAB program that implements this second-order asymmetric split-step Fourier method of Eq. (30) is given in its entirety as a function `hme_ssfm2` in Appendix A. The parameters that are given in set 1 have been shown to lead to a stable pulse [4]. Figure 1(a) shows the buildup of a stable mode-locked pulse from an initial small pulse $u_0(t) = 0.25\exp[-(t/5)^2]$ when $h = 0.04$.

As shown in Fig. 1(a), a similar evolution profile can be obtained if a second-order Runge–Kutta method is used to approximate the nonlinear integration in Eq. (29). However, to obtain higher accuracy and stability of the split-step method, one should use the analytical solution whenever it is available to evaluate the nonlinear integration. We found that the split-step method admits an enlarged stability region when the analytical solution is used by comparison to the case when a second-order Runge–Kutta method is used. The results are shown in Appendix B.

By comparison, the split-step method becomes unstable when we use the scheme of Eq. (17) if the nonlinear integration is evaluated explicitly. An example using the same step size is shown in Fig. 1(b). Here, the nonlinear step is handled

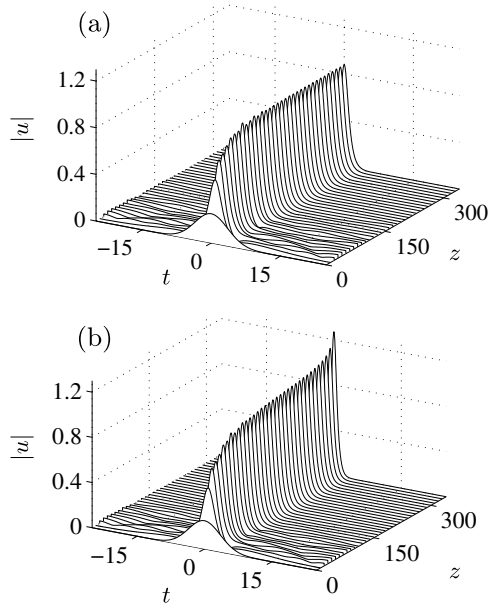

Fig. 1. Solving the HME starting from a small pulse $u_0(t) = 0.25\exp[-(t/5)^2]$ using set 1 in Table 1 with a step size $h = 0.04$: (a) The pulse evolves to a mode-locked pulse using the asymmetric splitting of Eq. (24) and (b) the pulse energy grows exponentially using the symmetric splitting scheme given in Eq. (17), where the nonlinear integration is evaluated using a second-order Runge–Kutta method.

by a second-order Runge–Kutta method since the analytical solution is not available. This code is also given as a MATLAB function `solveHME_ssfm_unstable` in Appendix A. Instead of evolving to a stable pulse, the initial pulse $u_0(t)$ grows exponentially and eventually blows up. This result is consistent with our earlier statement that explicit integration of the term that contains the saturated gain should be avoided.

4. ADDITIVE RUNGE–KUTTA METHODS

Another general approach that is often used to solve equations of the form of Eq. (1) is to solve the stiff part of the equation with an implicit method and the nonstiff part with an explicit method. These methods are called additive, implicit–explicit, or semi-implicit methods. Different approaches are used on the explicit and implicit parts. A good overview of many of these methods is presented by Ascher and co-workers [23,24]. Here, we implement the fourth-order ARK method of Kennedy and Carpenter [14]. In addition to fourth-order output, this method also gives a third-order output from which the local error can be estimated and the step size controlled. An extension to this method was recently used by Williams *et al.* [25] to simulate a waveguide array mode-locked laser using a PDE similar to the HME.

The basic idea of the ARK methods is to split Eq. (7) into two parts—one stiff and the other nonstiff—and to solve the stiff part with a diagonally implicit Runge–Kutta scheme and the nonstiff part with an explicit Runge–Kutta scheme. The full method can be written as

$$k_1 = u_k, \tag{34a}$$

$$k_i = u_k + h\sum_{j=1}^{i-1}[a_{ij}^{\mathrm{s}}F_{\mathrm{s}}(k_j) + a_{ij}^{\mathrm{ns}}F_{\mathrm{ns}}(k_j)] + h\gamma_{\mathrm{rk}}F_{\mathrm{s}}(k_i), \quad i \geq 2, \tag{34b}$$

$$u_{k+1} = u_k + h\sum_{i=1}^{m} b_i^{\mathrm{s}}F_{\mathrm{s}}(k_i) + h\sum_{i=1}^{m} b_i^{\mathrm{ns}}F_{\mathrm{ns}}(k_i), \tag{34c}$$

where F_{ns} is the nonstiff part of the ODE, F_{s} is the stiff part of the ODE, m is the number of stages, and k_i is the ith stage of the ARK method. The values of the coefficients a_{ij}^{s}, a_{ij}^{ns}, γ_{rk}, b_i^{s}, and b_i^{ns} are given in [14].

In each implicit stage $i = 2, \ldots, m$, we solve a nonlinear algebraic system. A complication here is that the nonlinear operator $g(\mathbf{u})$ is not differentiable in $\mathbf{u}$ because the complex conjugate of $\mathbf{u}$ explicitly appears. Hence, in order to solve the nonlinear system, we split the system into real and imaginary parts and form an extended system of $2N$ equations after discretization. So we write $\mathbf{q} = [\mathrm{Re}(\mathbf{u}), \mathrm{Im}(\mathbf{u})]^T$, and following Eq. (34b), $\mathbf{q}_i$ is solved at the ith stage ($i \geq 2$) from the nonlinear equation

$$h\sum_{j=1}^{i-1}[a_{ij}^{\mathrm{s}}\mathsf{F}_{\mathrm{s}}(\mathbf{q}_j) + a_{ij}^{\mathrm{ns}}\mathsf{F}_{\mathrm{ns}}(\mathbf{q}_j)] = \mathbf{q}_i - h\gamma_{\mathrm{rk}}\mathsf{F}_{\mathrm{s}}(\mathbf{q}_i), \tag{35}$$

where

$$\mathsf{F}_{\mathrm{s}}(\mathbf{q}) = [\hat{\mathsf{L}}\mathbf{q} + \hat{g}(\mathbf{q})\hat{\mathsf{K}}\mathbf{q}] \qquad \mathsf{F}_{\mathrm{ns}}(\mathbf{q}) = \begin{bmatrix} \mathrm{Re}\{(\delta + i\gamma)|\mathbf{u}|^2\mathbf{u}\} \\ \mathrm{Im}\{(\delta + i\gamma)|\mathbf{u}|^2\mathbf{u}\} \end{bmatrix},$$

and the linear operators of this extended system become the block matrices

$$\hat{\mathsf{L}} = \begin{bmatrix} \mathrm{Re}(\mathsf{L}) & -\mathrm{Im}(\mathsf{L}) \\ \mathrm{Im}(\mathsf{L}) & \mathrm{Re}(\mathsf{L}) \end{bmatrix}, \qquad \hat{\mathsf{K}} = \begin{bmatrix} \mathrm{Re}(\mathsf{K}) & -\mathrm{Im}(\mathsf{K}) \\ \mathrm{Im}(\mathsf{K}) & \mathrm{Re}(\mathsf{K}) \end{bmatrix}, \tag{36}$$

where in the case of the HME, the operators L and K are defined in Eq. (31). Meanwhile, the gain function in the extended system $\hat{g}$ is given in terms of $\mathbf{q}$ as

$$\hat{g}(\mathbf{q}) = \frac{g_0}{1 + \mathbf{q}^T\mathbf{q}/E_0}. \tag{37}$$

The Jacobian of the implicit stage system is therefore given by

$$\mathsf{J}_{\mathrm{ext}} = \mathsf{I} - h\gamma_{\mathrm{rk}}\left[\hat{\mathsf{L}} + \hat{g}(\mathbf{q})\hat{\mathsf{K}} - 2\frac{\hat{g}(\mathbf{q})^2}{g_0E_0}\hat{\mathsf{K}}\mathbf{q}\mathbf{q}^T\right]. \tag{38}$$

The matrix $\mathbf{q}\mathbf{q}^T$ appearing in Eq. (38) is a dense $2N \times 2N$ matrix. Directly solving the nonlinear system is not feasible; however, the matrix $\mathsf{J}_{\mathrm{ext}}$ is the sum of a block-diagonal matrix and a rank-one matrix. Hence, the matrix $\mathsf{J}_{\mathrm{ext}}$ can be inverted efficiently using the Sherman–Morrison formula [25,26], which gives the inverse of a matrix $\mathsf{A} + \mathbf{a}\mathbf{b}^T$ as

$$(\mathsf{A} + \mathbf{a}\mathbf{b}^T)^{-1} = \mathsf{A}^{-1} - \frac{\mathsf{A}^{-1}\mathbf{a}\mathbf{b}^T\mathsf{A}^{-1}}{1 + \mathbf{b}^T\mathsf{A}^{-1}\mathbf{a}}. \tag{39}$$

At each stage, we can apply this formula to Eq. (38) identifying

$$\mathsf{A} = \hat{\mathsf{L}} + \hat{g}(\mathbf{q})\hat{\mathsf{K}}, \qquad \mathbf{a} = -2\frac{\hat{g}(\mathbf{q})}{g_0 E_0}\hat{\mathsf{K}}\mathbf{q}, \quad \text{and} \quad \mathbf{b} = \mathbf{q}.$$

5. EXPONENTIAL TIME-DIFFERENCING RUNGE–KUTTA METHODS

Exponential time-differencing methods have been shown to be an efficient class of methods to solve many types of nonlinear wave equations. The exponential time-differencing methods have a long history and have been developed independently in several different fields [27,28]. We implement the fourth-order exponential time-differencing Runge–Kutta (ETDRK) scheme developed by Cox and Mathews [15]; however, we note that the ETDRK methods were not intended to solve problems of the form of Eq. (1) because the methods require exponentials of the integrals of the stiff operators to be calculated and are most efficient if these exponentials are only calculated once. Furthermore, the stiff operators are required to be linear so that their integrals in z can be calculated analytically.

To apply the ETDRK method to the HME, we split the problem into a linear stiff term and a nonlinear term with a reduced stiffness. This approach uses a constant approximation to the stiff nonlinear piece, which may then be integrated analytically. The remainder is included with the nonstiff piece. We may then write

$$\frac{\partial \mathbf{u}}{\partial z} = \{\mathsf{L} + g(\mathbf{u}_k)\mathsf{K}\}\mathbf{u} + \{[g(\mathbf{u}) - g(\mathbf{u}_k)]\mathsf{K}\mathbf{u} + \mathsf{N}(\mathbf{u}, z)\}. \tag{40}$$

The operators in both braces are stiff; however, during a single numerical step, the quantity $|g(\mathbf{u}) - g(\mathbf{u}_k)|$ is small compared to $g(\mathbf{u}_k)$, and in this case the second brace will be less stiff than the first operator. The implementation of the second brace of Eq. (40) requires that the nonlinear operator be evaluated in both the Fourier domain and the time domain, so that both a FFT and inverse FFT are required in order to evaluate the second brace.

A fourth-order ETDRK scheme is implemented in the following way [29]:

$$\mathbf{a}_k = \exp(\hat{L}h/2)\mathbf{u}_k + \hat{L}^{-1}[\exp(\hat{L}h/2) - \mathsf{I}]\hat{N}(\mathbf{u}_k, z_k), \tag{41a}$$

$$\mathbf{b}_k = \exp(\hat{L}h/2)\mathbf{u}_k + \hat{L}^{-1}[\exp(\hat{L}h/2) - \mathsf{I}]\hat{N}(\mathbf{a}_k, z_k + h/2), \tag{41b}$$

$$\mathbf{c}_k = \exp(\hat{L}h/2)\mathbf{a}_k + \hat{L}^{-1}[\exp(\hat{L}h/2) - \mathsf{I}][2\hat{N}(\mathbf{b}_k, z_k + h/2) - \hat{N}(\mathbf{u}_k, z_k)], \tag{41c}$$

$$\begin{aligned}\mathbf{u}_{k+1} = {} & \exp(\hat{L}h)\mathbf{u}_k + h^{-2}\hat{L}^{-3}\{[-4\mathsf{I} - \hat{L}h \\ & + \exp(\hat{L}h)(4\mathsf{I} - 3\hat{L}h + (\hat{L}h)^2)]\hat{N}(\mathbf{u}_k, z_k) \\ & + 2[2\mathsf{I} + \hat{L}h + \exp(\hat{L}h)(-2\mathsf{I} + \hat{L}h)] \\ & \times [\hat{N}(\mathbf{a}_k, z_k + h/2) + \hat{N}(\mathbf{b}_k, z_k + h/2)] \\ & + [-4\mathsf{I} - 3\hat{L}h - (\hat{L}h)^2 + \exp(\hat{L}h)(4\mathsf{I} - \hat{L}h)]\hat{N}(\mathbf{c}_k, z_k + h)\},\end{aligned} \tag{41d}$$

where I is the identity matrix, and the operators are defined as

$$\hat{L} = \mathsf{L} + g(\mathbf{u}_k)\mathsf{K}, \tag{42a}$$

$$\hat{N} = [g(\mathbf{u}) - g(\mathbf{u}_k)]\mathsf{K}\mathbf{u} + \mathsf{N}(\mathbf{u}, z). \tag{42b}$$

An additional difficulty is that the coefficients in Eq. (41) must be updated at each step, reducing the efficiency of the method. To calculate the coefficients, a numerical contour integral can be used to avoid round-off errors in the formula for small values of the linear operator [29]. This approach is too slow to be performed at each step, and we found that applying Padé approximants to the exponentials works well [30].

6. RESULTS

We test all the methods discussed in this paper to the HME using the two sets of parameters given in Table 1. In each case, the number of time points is $N = 1024$. We assume periodic boundary conditions in t. We use the same initial condition as in Section 3, $u_0(t) = 0.25\ \exp[-(t/5)^2]$, corresponding to an initial pulse that has a small amplitude compared to the mode-locked pulse. To estimate the error, we use a more accurate numerical solution $\mathbf{u}_r$ computed with a step size that is one quarter of the next smallest step size. Writing $\mathbf{u}^h$ for the evolution result with the step size h, the relative error is then calculated as

$$E_{\text{rel}}(h) = \frac{\|\mathbf{u}^h(z) - \mathbf{u}_r(z)\|_2}{\|\mathbf{u}_r(z)\|_2}, \tag{43}$$

where $\|\mathbf{u}\|_2 = \sqrt{\mathbf{u}^H\mathbf{u}}$. The results are summarized in Figs. 2 and 3. In both figures, the numerical methods that we use are denoted as follows: SSFM(s)2 is the second-order Richardson extrapolated version of the symmetric split-step method based on Eqs. (15) and (16), SSFM2 is the split-step Fourier method of Eq. (24), SSFM4 is the fourth-order Richardson extrapolated version of the SSFM2, ARK is the additive Runge–Kutta method of Section 4, and ETDRK is the ETDRK algorithm of Section 5.

Figures 2(a) and 3(a) show the computed relative error versus the step size that is used. Figures 2(b) and 3(b) show the computational time versus the relative error that is calculated using Eq. (43). We obtain all numerical results with code that was written in MATLAB and that runs on a desktop PC with a 2.93 GHz Intel Core2 Duo CPU.

From the results, for both parameter sets shown in Figs. 2 and 3, we find that the computational performance of the SSFM(s)2 and SSFM2 methods are similar. For a given step size, the SSFM(s)2 method generally has a smaller error at levels $<10^{-1}$ in set 1 and at levels $<10^{-2}$ in set 2. We attribute the better error performance of SSFM(s)2 to the use of Richardson extrapolation, which provides a better approximation to the saturated gain than does the method SSFM2. However, the method SSFM2 is more computationally efficient since it costs equal or less CPU time at almost all error levels $<10^{0}$. This advantage will be more significant as the evolution distance grows.

From the results for set 1 shown in Fig. 2, the ARK and ETDRK methods have similar errors for a given step size. The SSFM4 method has a smaller error, which we attribute to the use of the analytical solution in the nonlinear step.

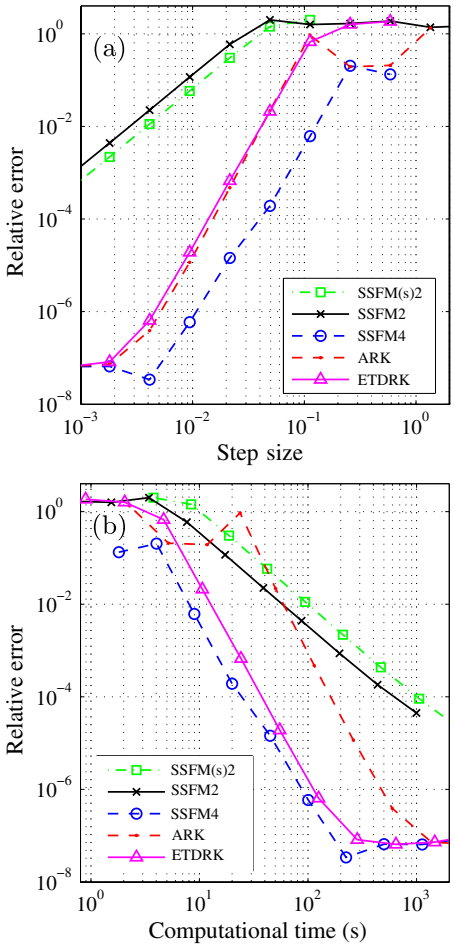

Fig. 2. (a) Relative error versus the step size and (b) the relative error versus the computational time. The HME of the Eq. (2) computation was solved with an initial small pulse up to $z = 300$ using set 1 in Table 1.

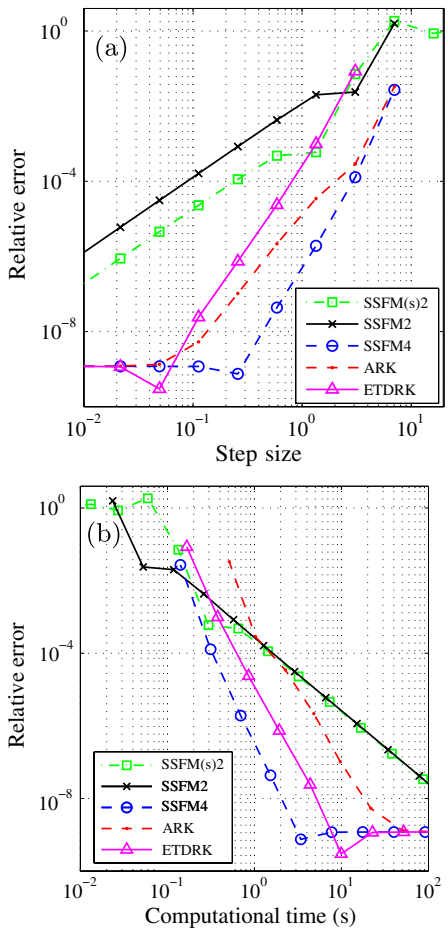

Fig. 3. (a) Relative error versus the step size and (b) the relative error versus the computational time. The HME of the Eq. (2) computation was solved with an initial small pulse up to $z = 300$ using set 2 in Table 1.

The SSFM4 method has a smaller error than the ETDRK method for a given step size and also performs better in computational efficiency. All methods appear to be stable in the range of step sizes of interest, and no method becomes unstable below the error level 10^{-1}. All of the fourth-order methods are significantly more efficient than the second-order method when the relative error is below 10^{-1}. Finally, we note that the ARK method takes significantly more time than the other fourth-order methods for the same relative error. There are two reasons for this result: First, a nonlinear system must be solved at each step, and second, the system is split into real and imaginary parts and is therefore twice the size. We do not take advantage of the fact that this system is now real, as MATLAB does not have that ability; however, we note that if coded in a language that allows further optimization, then the performance of the ARK method relative to other methods might be improved.

In the case of set 2 shown in Fig. 3, we find that the SSFM4 and ARK methods have similar errors at the same step size for relative errors above about 10^{-4}; however, below this value, the SSFM4 has a smaller relative error, and the error decreases at a slightly greater rate than $\mathcal{O}(h^4)$. We note that the ETDRK method becomes unstable for step sizes greater than $h = 4$, although with this step size the error is approaching the order 10^0, and therefore the step sizes are not of practical interest. The computational efficiencies of the methods using this parameter set are similar to the efficiencies of the methods using set 1.

7. CONCLUSION

In this paper, we have discussed the use of the split-step Fourier method, the ARK, and the ETDRK methods for solving the initial value problem for the HME. The ETDRK method performed better than expected even though it is not well suited to this problem. It requires the evaluation of the nonlinear operator in both the time and Fourier domains, and the coefficients of the method must be recalculated at each step.

The ARK method was stable over a large range of parameters as all stiff terms were treated implicitly. In addition, it is a well-established method. The disadvantages of the ARK method are that it is complicated to program, and it requires splitting the implicit problem into real and imaginary parts.

The asymmetric split-step Fourier method has been shown to be easy to program and computationally efficient. When Richardson extrapolation was used to yield a fourth-order method, the asymmetric split-step scheme was found to be the most computationally efficient method for solving the HME for errors below 10^{-2}.

APPENDIX A: MATLAB CODES

The following is the MATLAB code to solve the HME with the split-step Fourier method of Eq. (24). The code is used to create the plot of Fig. 1(a).

```
function hme_ssfm2()
% The equation parameters
g0 = 0.4; PsatTR = 1; loss = 0.2;
Omega = sqrt(10); del = 0.03;
gam = 4; beta2 = -2;
% Discretization
Nt = 1024; T = 50; dt = T/Nt;
t = (-Nt/2:1:Nt/2 - 1)' * dt;
dw = 2 * pi/T; w = [0:Nt/2 - 1   0   -Nt/2 + 1: - 1]' * dw;
Z = 400; h = 0.04; NumSteps = round(Z/h);
SaveInterval = 250;
% Operators
L = (1i * beta2 * w.^2 - loss)/2;
K = (1 - (w/Omega).^2)/2;
% Initial condition
u0 = 0.25 * exp(-(t/5).^2);
uf = fft(u0); uplot = abs(u0).';
zplot = 0; Psatf = PsatTR/dt * Nt;
for istep = 1:NumSteps
  g1 = g0/(1 + norm(uf)^2/Psatf);
  g2 = -2 * (g1^2/g0/Psatf) * ...
    real(dot(uf, (L + g1 * K). * uf));
  u = ifft(exp(L * h/2 + (g1 * h/2 + g2/8 * h^2) * K). * uf);
  uf = fft(exp(-(del + 1i * gam)/(2 * del)...
    * log(1 - 2 * del * h * abs(u).^2)). * u);
  g1 = g0/(1 + norm(uf)^2/Psatf);
  uf = exp(L * h/2 + (g1 * h/2 + g2/8 * h^2) * K). * uf;
  if mod(istep, SaveInterval) == 0
    uplot = [uplot; abs(ifft(uf)).'];
    zplot = [zplot, istep * h];
  end
end
waterfall(t, zplot, uplot); colormap([0 0 0]);
view(30, 30); xlabel('t'); ylabel('z');
end
```

The following is the MATLAB code to solve the HME with the split-step Fourier method of Eq. (17), where the nonlinear integration is evaluated by a second-order Runge–Kutta method. The code is used to create the plot of Fig. 1(b).

```
function SolveHME_SSFM_unstable()
% The equation parameters
g0 = 0.4; PsatTR = 1; loss = 0.2;
Omega = sqrt(10); del = 0.03;
gam = 4; beta2 = -2;
% Discretization
Nt = 1024; T = 50; dt = T/Nt;
t = (-Nt/2:1:Nt/2 - 1)' * dt;
dw = 2 * pi/T; w = [0:Nt/2 - 1   0   -Nt/2 + 1: - 1]' * dw;
Z = 400; h = 0.04; NumSteps = round(Z/h);
SaveInterval = 250;
% Operators
L = (1i * beta2 * w.^2 - loss)/2;
K = (1 - (w/Omega).^2)/2;
% Initial condition
u0 = 0.25 * exp(-(t/5).^2);
uf = fft(u0); uplot = u0.'; zplot = 0;
Psatf = PsatTR/dt * Nt;
for istep = 1:NumSteps
```

(Table continued)

Continued

```
  uf = exp(L * h/2). * uf;
  uf = RungeKutta2(uf, h, g0, Psatf, del, gam, K);
  uf = exp(L * h/2). * uf;
  if any(isnan(uf))
    break;
  end
  if mod(istep, SaveInterval) == 0
    uplot = [uplot; ifft(uf).'];
    zplot = [zplot, istep * h];
  end
end
waterfall(t, zplot, abs(uplot));
colormap([0 0 0]); view(30, 30);
xlabel('t'); ylabel('z'); axis tight;
end
function uf_out = RungeKutta2 (uf, h, g0, Psatf,...
del, gam, K)
k1 = 0.5 * h * gKu_Nu(uf, g0, Psatf, del, gam, K);
k2 = h * gKu_Nu(uf + k1, g0, Psatf, del, gam, K);
uf_out = uf + k2;
end
function dudt = gKu_Nu(uf, g0, Psatf, del, gam, K)
g = g0/(1 + norm(uf)^2/Psatf);
u = ifft(uf);
dudt = g * K. * uf + fft((del + 1i * gam) * abs(u).^2. * u);
end
```

APPENDIX B: STABILITY OF THE SPLIT-STEP METHOD

Handling the nonlinear step $\int_0^h \mathcal{N}(u,z')\mathrm{d}z'$ analytically instead of explicitly not only reduces the computation error but also enlarges the region of stability. We consider the following scalar ODE:

$$\frac{\mathrm{d}u}{\mathrm{d}z} = cu + (\delta + i\gamma)|u|^2 u, \tag{B1}$$

where $u(z)$ is a function of z. The coefficients δ and γ are real constants. Equation (B1) is similar to Eq. (2), but it has a reduced complexity in which the dependence of u on t is not considered, and the loss, the band-limited gain, and the dispersion are lumped into a constant c. In this case, we have $\mathcal{N}(u,z) = (\delta + i\gamma)|u|^2 u$.

We now apply the standard symmetric split-step method of Section 2.A to Eq. (B1), and we define the absolute stability parameter σ_N of each step as

$$\sigma_N = \frac{u_{k+1}}{u_k}. \tag{B2}$$

The split-step scheme is stable if $|\sigma_N| < 1$. If a second-order Runge–Kutta method is applied to handle $\mathcal{N}(u,z)$, we find in the $(k+1)$th step

$$u_{k+1} = \exp(C)[1 + (A + iB)|D|^2 D\exp(C)]u_k, \tag{B3}$$

where $D = 1 + (A + iB)\exp(C)/2$, $A = h\delta|u_k|^2$, $B = h\gamma|u_k|^2$, and $C = hc$. We thus find

$$\sigma_N = \exp(C)[1 + (A + iB)|D|^2 D\exp(C)]. \tag{B4}$$

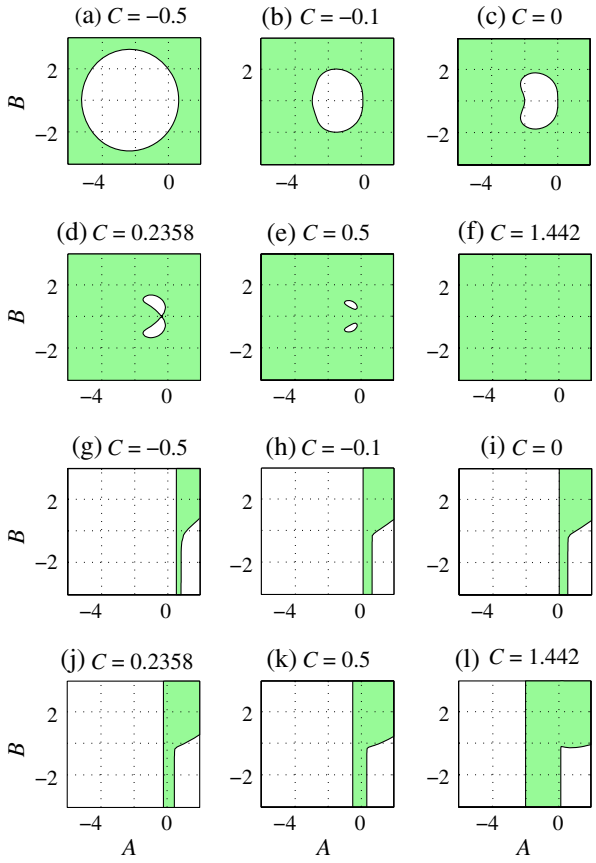

Fig. 4. Stability regions of the split-step method applying to Eq. (B1). The white regions indicate stability. (a)–(f) show the cases in which $\mathcal{N}(u,z)$ is handled explicitly and (g)–(l) show the cases in which $\mathcal{N}(u,z)$ is handled analytically.

By comparison, for the case when $\mathcal{N}(u,z)$ is handled analytically using Eq. (29), we obtain

$$\sigma_N = \exp\left\{C - \frac{A+iB}{2A}\log[1-2A\exp(C)]\right\}, \tag{B5}$$

if $A \neq 0$. When $A = 0$, we simply have $\sigma_N = \exp(C)$.

The stability regions as A, B, and C vary are shown in Fig. 4. The complex plane is defined in terms of $A + iB$, and different values of C are noted above each subfigure. The white regions mark the stable regions for the method. Figures 4(a)–4(f) show the cases when $\mathcal{N}(u,z)$ is handled by the Runge–Kutta method. Each stable region in this case is symmetric about the A axis, which implies that σ_N is an even function of A, which can be proved by expanding σ_N in a Taylor series in A and B using Eq. (B4). Also, the stability region shrinks as C increases from being negative to positive, i.e., when a transitions occurs from loss to gain. The region starts from a finite continuous region on the complex plane. Then, it gradually shrinks and breaks into two symmetric pieces around $C = 0.2358$, until it finally vanishes around $C = 1.442$.

By contrast, Figs. 4(g)–4(l) are for the cases where $\mathcal{N}(u,z)$ is handled analytically. In each subfigure, the stability region is separated, where one piece is bounded to the right by some value of A, while the other piece is on the lower-right portion of the complex plane that implies $1 - 2A\exp(C) < 0$, which corresponds to the pulse power $|u|^2$ being negative. This latter case is nonphysical and not of concern. The special case $A = 0$ implies that the algorithm is unstable unless $C < 0$. The stability boundary shrinks to the left as C increases.

By comparison, we show the stable regions are significantly enlarged when the nonlinear integration $\int_0^h \mathcal{N}(u,z')\mathrm{d}z'$ is evaluated analytically than in the cases when a second-order Runge–Kutta method is used. We conclude that in order to obtain good performance for both accuracy and stability, it is preferable to evaluate this nonlinear step using its analytical form, if available.

ACKNOWLEDGMENTS

This work was supported in part by the Office of Naval Research. We would like to acknowledge useful discussions with John Zweck in the writing of this paper. All codes used to plot the results found in this paper are available at the website http://photonics.umbc.edu/software.

REFERENCES

1. O. V. Sinkin, R. Holzlöhner, J. Zweck, and C. R. Menyuk, "Optimization of the split-step Fourier method in modeling optical-fiber communications systems," J. Lightwave Technol. **21**, 61–68 (2003).
2. S. A. Diddams, "The evolving optical frequency comb [invited]," J. Opt. Soc. Am. B **27**, B51–B62 (2010).
3. H. A. Haus, "Theory of mode locking with a fast saturable absorber," J. Appl. Phys. **46**, 3049–3058 (1975).
4. T. Kapitula, J. N. Kutz, and B. Sandstede, "Stability of pulses in the master mode-locking equation," J. Opt. Soc. Am. B **19**, 740–746 (2002).
5. C. R. Menyuk, J. K. Wahlstrand, J. Willits, R. P. Smith, T. R. Schibli, and S. T. Cundiff, "Pulse dynamics in mode-locked lasers: relaxation oscillations and frequency pulling," Opt. Express **15**, 6677–6689 (2007).
6. M. Shtaif, C. R. Menyuk, M. L. Dennis, and M. C. Gross, "Carrier-envelope phase locking of multipulse lasers with an intracavity Mach–Zehnder interferometer," Opt. Express **19**, 23202–23214 (2011).
7. A. Hasegawa and F. Tappert, "Transmission of stationary nonlinear optical pulses in dispersive dielectric fibers. II. Normal dispersion," Appl. Phys. Lett. **23**, 171–172 (1973).
8. A. Ablowitz and P. Clarkson, *Solitons, Nonlinear Evolution Equations and Inverse Scattering*, London Mathematical Society Lecture Note Series (Cambridge University, 1991).
9. B. Fornberg and T. A. Driscoll, "A fast spectral algorithm for nonlinear wave equations with linear dispersion," J. Comput. Phys. **155**, 456–467 (1999).
10. L. Trefethen, *Spectral Methods in MATLAB*, Software, Environments and Tools Series (Cambridge University, 2000).
11. R. J. LeVeque, *Finite Difference Methods for Ordinary and Partial Differential Equations* (Society for Industrial and Applied Mathematics, 2007).
12. A. Iserles, *A First Course in the Numerical Analysis of Differential Equations*, Cambridge Texts in Applied Mathematics (Cambridge University, 1996).
13. G. Bosco, A. Carena, V. Curri, R. Gaudino, P. Poggiolini, and S. Benedetto, "Suppression of spurious tones induced by the split-step method in fiber systems simulation," IEEE Photon. Technol. Lett. **12**, 489–491 (2000).
14. C. A. Kennedy and M. H. Carpenter, "Additive Runge–Kutta schemes for convection-diffusion-reaction equations," Appl. Numer. Math. **44**, 139–181 (2003).
15. S. Cox and P. Matthews, "Exponential time differencing for stiff systems," J. Comput. Phys. **176**, 430–455 (2002).
16. G. Strang, "On the construction and comparison of difference schemes," SIAM J. Numer. Anal. **5**, 506–517 (1968).
17. K. Bagrinovskii and S. Godunov, "Difference schemes for multi-dimensional problems," Doklady Akademii Nauk **115**, 431–433 (1957).

18. H. Yoshida, "Construction of higher order symplectic integrators," Phys. Lett. A **150**, 262–268 (1990).
19. J. Boyd, *Chebyshev and Fourier Spectral Methods*, Dover Books on Mathematics (Dover Publications, 2001).
20. G. Agrawal, *Nonlinear Fiber Optics*, *Optics and Photonics* (Elsevier, 2010).
21. L. F. Richardson, "The approximate arithmetical solution by finite differences of physical problems involving differential equations, with an application to the stresses in a masonry dam," Proc. R. Soc. A **210**, 307–357 (1911).
22. J. Kutz, "Mode-locked soliton lasers," SIAM Rev. **48**, 629–678 (2006).
23. U. M. Ascher, S. J. Ruuth, and B. T. R. Wetton, "Implicit–explicit methods for time-dependent partial differential equations," SIAM J. Numer. Anal. **32**, 797–823 (1995).
24. U. Ascher and L. Petzold, *Computer Methods for Ordinary Differential Equations and Differential-Algebraic Equations*, Miscellaneous Titles in Applied Mathematics Series (Society for Industrial and Applied Mathematics, 1998).
25. M. O. Williams, J. Wilkening, E. Shlizerman, and J. N. Kutz, "Continuation of periodic solutions in the waveguide array mode-locked laser," Physica D **240**, 1791–1804 (2011).
26. J. Nocedal and S. Wright, *Numerical Optimization*, Springer Series in Operations Research (Springer, 2006).
27. A. Taflove and S. Hagness, *Computational Electrodynamics: The Finite-Difference Time-Domain Method*, Artech House Antennas and Propagation Library (Artech House, 2005).
28. D. R. Mott, E. S. Oran, and B. van Leer, "A quasi-steady-state solver for the stiff ordinary differential equations of reaction kinetics," J. Comput. Phys. **164**, 407–428 (2000).
29. A. Kassam and L. Trefethen, "Fourth-order time-stepping for stiff PDEs," SIAM J. Sci. Comput. **26**, 1214–1233 (2005).
30. H. Berland, B. Skaflestad, and W. M. Wright, "EXPINT-a MATLAB package for exponential integrators," ACM Trans. Math. Softw. **33**, 4 (2007).